LUND UNIVERSITY

Physical limitations on metamaterials: restrictions on scattering and absorption over a frequency interval

Sohl, Christian; Gustafsson, Mats; Kristensson, Gerhard

2007

[Link to publication](#)

Total number of authors:
3

Physical limitations on metamaterials: Restrictions on scattering and absorption over a frequency interval

Christian Sohl, Mats Gustafsson, and Gerhard Kristensson

Christian Sohl, Mats Gustafsson, and Gerhard Kristensson
{Christian.Sohl,Mats.Gustafsson,Gerhard.Kristensson}@es.lth.se

Department of Electrical and Information Technology
Electromagnetic Theory
P.O. Box 118
SE-221 00 Lund
Sweden

Abstract

A limitation on the extinction cross section, valid for all scatterers satisfying some basic physical assumptions, is investigated. The physical limitation is obtained from the holomorphic properties of the forward scattering dyadic. The analysis focuses on the consequences for materials with negative permittivity and permeability, *i.e.*, metamaterials. From a broadband point of view, the limitations imply that there is no fundamental difference between metamaterials and ordinary materials with respect to scattering and absorption. The analysis is illustrated by three numerical examples of metamaterials modeled by temporal dispersion.

1 Introduction

Since the investigation of negative refractive index materials by V. G. Veselago in Ref. 14, there has been an enormous theoretical and experimental interest in the possibilities of such materials. These materials are often referred to as metamaterials, even though a metamaterial in general is a much broader concept of a structured material, and not necessarily composed of materials with negative permittivity and permeability values. Negative refractive index materials seem not to occur naturally, and if they can be manufactured, they possess extravagant properties promising for various physical applications, see Refs. 9 and 11, and references therein.

The scattering properties of obstacles consisting of metamaterials have been of considerable scientific interest during the last decade. Mostly canonical geometries, such as the spheres, see *e.g.*, Ref. 10, have been employed, and the design of scatterers that both increases and decreases the scattering properties have been reported.

The analysis presented in this paper shows that, from a broadband point of view, the scattering and absorption properties of any material (not just metamaterials) that satisfy basic physical assumptions, are limited by the static electric and magnetic behavior of the composed materials. In particular, we show that, when these limitations are applied to low-frequency resonances on metamaterials, large scattering effects have to be traded for bandwidth. Specifically, the lower the resonance frequency, the higher its Q-value. For a single frequency, metamaterials may possess exceptional characteristics, but, since bandwidth is essential, it is important to study metamaterials over a frequency interval, and with physically realistic dispersion models.

The results presented in this paper are independent of how the material that constitutes the scatterer is constructed or produced. This broad range of material models is a consequence of the fact that the analysis is solely based on the principles of energy conservation and causality applied to a set of linear and time-translational invariant constitutive relations.

The present paper is a direct application of the theory for broadband scattering introduced in Ref. 12. In addition to material modeling, the theory has also been applied successfully to physical limitations on arbitrary antennas in Refs. 1 and 3. The underlying mathematical description for broadband scattering is motivated by

the study of causality and dispersion relations in the scattering theory of waves and particles in Refs. 7 and 8.

2 Derivation of the integrated extinction

Consider a localized and bounded scatterer $V \subset \mathbb{R}^3$ of arbitrary shape. The dynamics of the material in V is modeled by the Maxwell equations with general heterogeneous and anisotropic constitutive relations. The constitutive relations are expressed in terms of the electric and magnetic susceptibility dyadics, $\boldsymbol{\chi}_{\mathrm{e}}$ and $\boldsymbol{\chi}_{\mathrm{m}}$, respectively. Due to the heterogeneous character of $\boldsymbol{\chi}_{\mathrm{e}}$ and $\boldsymbol{\chi}_{\mathrm{m}}$, V can be interpreted both as a single scatterer and as a set of multiple scatterers. The present analysis includes the perfectly conducting material model as well as general temporal dispersion with or without a conductivity term. The analysis can also be extended with minor changes to bianisotropic materials with the same conclusions drawn.

The direct scattering problem addressed in this paper is Fourier-synthesized plane wave scattering by V. Due to the linearity of the Maxwell equations, it is sufficient to consider monochromatic plane waves with time dependence $\mathrm{e}^{-\mathrm{i}\omega t}$. The incident wave is assumed to impinge in the $\hat{\boldsymbol{k}}$-direction with an electric field $\boldsymbol{E}_{\mathrm{i}}$ depending only on the difference $\tau = \mathrm{c}_0 t - \hat{\boldsymbol{k}} \cdot \boldsymbol{x}$, where $\boldsymbol{x}$ denotes the space variable. Introduce the far field amplitude $\boldsymbol{F}$ via $\boldsymbol{E}_{\mathrm{s}} = \boldsymbol{F}(\mathrm{c}_0 t - x, \hat{\boldsymbol{x}})/x + \mathcal{O}(x^{-2})$ as $x \to \infty$, where $\boldsymbol{E}_{\mathrm{s}}$ represents the scattered electric field. Under the assumption that the constitutive relations of V are linear and time-translational invariant, $\boldsymbol{F}$ is given by the convolution

$$\boldsymbol{F}(\tau, \hat{\boldsymbol{x}}) = \int_{-\infty}^{\infty} \mathbf{S}_{\mathrm{t}}(\tau - \tau', \hat{\boldsymbol{k}}, \hat{\boldsymbol{x}}) \cdot \boldsymbol{E}_{\mathrm{i}}(\tau') \, \mathrm{d}\tau'.$$

Here, $\mathbf{S}_{\mathrm{t}}$ is assumed to be primitive causal in the forward direction, $i.e.$, $\mathbf{S}_{\mathrm{t}}(\tau, \hat{\boldsymbol{k}}, \hat{\boldsymbol{k}}) = 0$ for $\tau < 0$, see Ref. 8. Furthermore, introduce the forward scattering dyadic $\mathbf{S}$ as the Fourier transform of $\mathbf{S}_{\mathrm{t}}$ evaluated in the forward direction, $i.e.$,

$$\mathbf{S}(k, \hat{\boldsymbol{k}}) = \int_{0^-}^{\infty} \mathbf{S}_{\mathrm{t}}(\tau, \hat{\boldsymbol{k}}, \hat{\boldsymbol{k}}) \mathrm{e}^{\mathrm{i}k\tau} \, \mathrm{d}\tau, \tag{2.1}$$

where $k = \omega/\mathrm{c}_0$. The extension of (2.1) to complex-valued k with $\mathrm{Im}\, k > 0$ improves the convergence of the integral and implies that $\mathbf{S}$ is holomorphic in the upper half of the complex k-plane. Recall that the cross symmetry relation $\mathbf{S}(k, \hat{\boldsymbol{k}}) = \mathbf{S}^*(-k^*, \hat{\boldsymbol{k}})$ is a direct consequence of such an extension.

Introduce $\boldsymbol{E}_0$ as the Fourier amplitude of the incident wave, and let $\hat{\boldsymbol{p}}_{\mathrm{e}} = \boldsymbol{E}_0/|\boldsymbol{E}_0|$ and $\hat{\boldsymbol{p}}_{\mathrm{m}} = \hat{\boldsymbol{k}} \times \hat{\boldsymbol{p}}_{\mathrm{e}}$ denote the associated electric and magnetic polarizations, respectively. Recall that $\boldsymbol{E}_0$ is subject to the constraint of transverse wave propagation, $i.e.$, $\boldsymbol{E}_0 \cdot \hat{\boldsymbol{k}} = 0$. Under the assumption that $\hat{\boldsymbol{p}}_{\mathrm{e}}$ and $\hat{\boldsymbol{p}}_{\mathrm{m}}$ are independent of k, it follows from the analysis above that also $\varrho(k) = \hat{\boldsymbol{p}}_{\mathrm{e}}^* \cdot \mathbf{S}(k, \hat{\boldsymbol{k}}) \cdot \hat{\boldsymbol{p}}_{\mathrm{e}}/k^2$ is holomorphic for $\mathrm{Im}\, k > 0$. Cauchy's integral theorem applied to ϱ then yields, see Ref. 12,

$$\varrho(\mathrm{i}\varepsilon) = \int_0^\pi \frac{\varrho(\mathrm{i}\varepsilon - \varepsilon\mathrm{e}^{\mathrm{i}\phi})}{2\pi} \, \mathrm{d}\phi + \int_0^\pi \frac{\varrho(\mathrm{i}\varepsilon + R\mathrm{e}^{\mathrm{i}\phi})}{2\pi} \, \mathrm{d}\phi + \int_{\varepsilon < |k| < R} \frac{\varrho(k + \mathrm{i}\varepsilon)}{2\pi\mathrm{i}k} \, \mathrm{d}k. \tag{2.2}$$

Here, it is assumed that ϱ is sufficiently regular to extend the contour to the real-axis in the last integral on the right hand side of (2.2). Relation (2.2) is subject to the limits $\varepsilon \to 0$ and $R \to \infty$.

The long wavelength limit of ϱ on the left hand side of (2.2) and the integrand in the first integral on the right hand side can be derived from a power series expansion of the Maxwell equations. The result is, see Ref. 4,

$$\varrho(\varepsilon) = \frac{1}{4\pi} \left(\hat{\boldsymbol{p}}_\mathrm{e}^* \cdot \boldsymbol{\gamma}_\mathrm{e} \cdot \hat{\boldsymbol{p}}_\mathrm{e} + \hat{\boldsymbol{p}}_\mathrm{m}^* \cdot \boldsymbol{\gamma}_\mathrm{m} \cdot \hat{\boldsymbol{p}}_\mathrm{m} \right) + \mathcal{O}(\varepsilon) \tag{2.3}$$

as $\varepsilon \to 0$, where $\boldsymbol{\gamma}_\mathrm{e}$ and $\boldsymbol{\gamma}_\mathrm{m}$ denote the electric and magnetic polarizability dyadics, respectively. For the appropriate definitions of $\boldsymbol{\gamma}_\mathrm{e}$ and $\boldsymbol{\gamma}_\mathrm{m}$, and some of their properties, see Ref. 12 and references therein.

The second integral on the right hand side of (2.2) vanishes in the limit as $R \to \infty$ according to the extinction paradox in Ref. 13. In terms of ϱ, a generalization of the extinction paradox states that $\varrho(k) = -A/(2\pi i k) + \mathcal{O}(|k|^{-2})$ as $|k| \to \infty$. The constant A is real-valued since $\mathbf{S}(\mathrm{i}k, \hat{\boldsymbol{k}})$ is real-valued for real-valued k. For a large class of scatterers, A coincides with the projected area in the forward direction. The disappearance of the second integral on the right hand side of (2.2) is also supported by the fact that the high-frequency response of a material is non-unique from a modeling point of view, see Ref. 2.

From the details above, it is clear that the real part of (2.2) when subject to the limits $\varepsilon \to 0$ and $R \to \infty$, yields

$$\varrho(0) = \frac{1}{2}\varrho(0) + \frac{1}{8\pi^2} \int_{-\infty}^{\infty} \frac{\sigma_\mathrm{ext}(k)}{k^2} \, \mathrm{d}k, \tag{2.4}$$

where the optical theorem $\sigma_\mathrm{ext}(k) = 4\pi k \operatorname{Im} \varrho(k)$ has been invoked, see Ref. 12. Here, the extinction cross section σ_ext is defined as the sum of the scattered and absorbed power divided by the power flow density of the incident wave. Recall that the optical theorem is a direct consequence of energy conservation, see Ref. 7. Relation (2.3) inserted into (2.4) using the wavelength variable $\lambda = 2\pi/k$ finally yields

$$\int_0^{\infty} \sigma_\mathrm{ext}(\lambda) \, \mathrm{d}\lambda = \pi^2 \left(\hat{\boldsymbol{p}}_\mathrm{e}^* \cdot \boldsymbol{\gamma}_\mathrm{e} \cdot \hat{\boldsymbol{p}}_\mathrm{e} + \hat{\boldsymbol{p}}_\mathrm{m}^* \cdot \boldsymbol{\gamma}_\mathrm{m} \cdot \hat{\boldsymbol{p}}_\mathrm{m} \right). \tag{2.5}$$

The left hand side of (2.5) is referred to as the integrated extinction. For additional details on the derivation of (2.5), see Ref. 12.

Relation (2.5) is slightly modified when an isotropic conductivity term $\mathrm{i}\varsigma/\omega\epsilon_0$ is introduced in $\boldsymbol{\chi}_\mathrm{e}$ for some region of V, see Ref. 12. The scalar conductivity ς is non-negative and assumed independent of ω. In the presence of a conductivity term, the analysis in Ref. 4 shows that the right hand side of (2.5) should be evaluated in the limit as the eigenvalues of $\boldsymbol{\chi}_\mathrm{e}$ approach infinity independently of $\boldsymbol{\chi}_\mathrm{m}$. The perfectly conducting case is obtained as the eigenvalues of $\boldsymbol{\chi}_\mathrm{m}$ in addition approach -1.

Electric and magnetic material properties are seen to be treated on equal footing in (2.5), both in terms of polarization and material description. Furthermore,

the right hand side of (2.5) depends solely on the long wavelength limit or static response of V, while the left hand side is a dynamic quantity which unites the scattering and absorption properties of V. Recall that $\boldsymbol{\gamma}_{\mathrm{e}}$ and $\boldsymbol{\gamma}_{\mathrm{m}}$ only are functions of the geometry of V and the long wavelength susceptibilities $\boldsymbol{\chi}_{\mathrm{e}}(0) = \lim_{\omega \to 0} \boldsymbol{\chi}_{\mathrm{e}}(\omega)$ and $\boldsymbol{\chi}_{\mathrm{m}}(0) = \lim_{\omega \to 0} \boldsymbol{\chi}_{\mathrm{m}}(\omega)$. Here, $\boldsymbol{\chi}_{\mathrm{e}}(0)$ and $\boldsymbol{\chi}_{\mathrm{m}}(0)$ are real-valued in the case of vanishing conductivity. For heterogeneous structures, the long wavelength susceptibilities $\boldsymbol{\chi}_{\mathrm{e}}(0)$ and $\boldsymbol{\chi}_{\mathrm{m}}(0)$ also depend on the space variable $\boldsymbol{x}$.

In many applications, the scatterer is randomly oriented with respect to an ensamble of incident waves. For this purpose, the averaged extinction cross section $\bar{\sigma}_{\mathrm{ext}}$ is conviniently introduced by averaging (2.5) over the unit sphere in $\mathbb{R}^3$, *i.e.*,

$$\int_0^\infty \bar{\sigma}_{\mathrm{ext}}(\lambda) \, \mathrm{d}\lambda = \frac{\pi^2}{3} \operatorname{trace}(\boldsymbol{\gamma}_{\mathrm{e}} + \boldsymbol{\gamma}_{\mathrm{m}}). \tag{2.6}$$

For non-spherical particles, (2.6) provides a neat verification of (2.5) without specifying the orientation of V with respect to the incident wave, see Sec. 4.1.

3 Bounds on scattering and absorption

For applications to exotic material models such as metamaterials, it is beneficial to introduce the high-contrast polarizability dyadic $\boldsymbol{\gamma}_\infty$ as the limit of either $\boldsymbol{\gamma}_{\mathrm{e}}$ or $\boldsymbol{\gamma}_{\mathrm{m}}$ when the eigenvalues of $\boldsymbol{\chi}_{\mathrm{e}}(0)$ or $\boldsymbol{\chi}_{\mathrm{m}}(0)$ simultaneously become infinitely large. From the variational properties of $\boldsymbol{\gamma}_{\mathrm{e}}$ and $\boldsymbol{\gamma}_{\mathrm{m}}$ discussed in Ref. 12 and references therein, it follows that both $\boldsymbol{\gamma}_{\mathrm{e}}$ and $\boldsymbol{\gamma}_{\mathrm{m}}$ are bounded from above by $\boldsymbol{\gamma}_\infty$, *i.e.*,

$$\int_0^\infty \sigma_{\mathrm{ext}}(\lambda) \, \mathrm{d}\lambda \le \pi^2 \left(\hat{\boldsymbol{p}}_{\mathrm{e}}^* \cdot \boldsymbol{\gamma}_\infty \cdot \hat{\boldsymbol{p}}_{\mathrm{e}} + \hat{\boldsymbol{p}}_{\mathrm{m}}^* \cdot \boldsymbol{\gamma}_\infty \cdot \hat{\boldsymbol{p}}_{\mathrm{m}} \right). \tag{3.1}$$

The right hand side of (3.1) is independent of any material properties, depending only on the geometry and the orientation of V with respect to the incident wave. The right hand side can, independent of $\hat{\boldsymbol{p}}_{\mathrm{e}}$ and $\hat{\boldsymbol{p}}_{\mathrm{m}}$, further be estimated from above by the eigenvalues of $\boldsymbol{\gamma}_\infty$, see Ref. 12.

The integrated extinction can be used to derive various bounds and variational principles for broadband scattering. Since the extinction cross section σ_{ext} by definition is non-negative, the left hand side of (2.5) can be estimated from below as

$$|\Lambda| \inf_{\lambda \in \Lambda} \sigma(\lambda) \le \int_\Lambda \sigma(\lambda) \, \mathrm{d}\lambda \le \int_0^\infty \sigma_{\mathrm{ext}}(\lambda) \, \mathrm{d}\lambda, \tag{3.2}$$

where $\Lambda \subset [0, \infty)$ denotes an arbitrary wavelength interval with absolute bandwidth $|\Lambda|$. Here, σ represents any of the scattering, absorption and extinction cross sections, see Ref. 12 for their appropriate definitions. The quantity $|\Lambda| \inf_{\lambda \in \Lambda} \sigma(\lambda)$ in (3.2) is particularly useful for box-shaped limitations, *viz.*,

$$|\Lambda| \inf_{\lambda \in \Lambda} \sigma(\lambda) \le \pi^2 \left(\hat{\boldsymbol{p}}_{\mathrm{e}}^* \cdot \boldsymbol{\gamma}_{\mathrm{e}} \cdot \hat{\boldsymbol{p}}_{\mathrm{e}} + \hat{\boldsymbol{p}}_{\mathrm{m}}^* \cdot \boldsymbol{\gamma}_{\mathrm{m}} \cdot \hat{\boldsymbol{p}}_{\mathrm{m}} \right). \tag{3.3}$$

From (3.2) and (3.3) it is clear that the long wavelength limit response of V also provides upper bounds on scattering and absorption within any finite wavelength

interval Λ. Analogous to (3.1), the right hand side of (3.3) can also be estimated from above by $\boldsymbol{\gamma}_\infty$ and its eigenvalues. An important consequence of the fact that (2.5) and (3.3) only depend on the long wavelength limit response of V is that they are independent of any temporal dispersion.

The fact that (2.5) and (3.3) are independent of any temporal dispersion implies that there is no fundamental difference in scattering and absorption (in a broadband sense) between metamaterials and ordinary materials, as long as the static properties of the material are identical. In fact, it is well known that passive materials must be temporally dispersive since the Kramers-Kronig relations imply that $\boldsymbol{\chi}_\mathrm{e}(0)$ and $\boldsymbol{\chi}_\mathrm{m}(0)$ element-wise are non-negative in the absence of a conductivity term, see Ref. 5. Recall that the Kramers-Kronig relations are a direct consequence of primitive causality, see Ref. 8.

When an isotropic conductivity term i$\varsigma/\omega\epsilon_0$ is present in $\boldsymbol{\chi}_\mathrm{e}$, the Kramers-Kronig relations must be modified due to the singular behavior of $\boldsymbol{\chi}_\mathrm{e}$. As mentioned above, the analysis in Ref. 4 shows that the introduction of such a term in $\boldsymbol{\chi}_\mathrm{e}$ implies that $\boldsymbol{\gamma}_\mathrm{e}$ should be substituted for $\boldsymbol{\gamma}_\infty$ in the right hand side of (2.5) and (3.3).

Two popular models for temporal dispersion for metamaterials are the Drude and Lorentz models, see (4.2) and Ref. 8, respectively. The Drude model is often preferred over the Lorentz model since it provides a wider bandwidth over which the eigenvalues of $\boldsymbol{\chi}_\mathrm{e}$ and $\boldsymbol{\chi}_\mathrm{m}$ attain values less than -1. However, based on the arguments above, it is uninteresting from the point of view of (2.5) and (3.3) which temporal dispersion model is used to characterize metamaterials as long as the model satisfies primitive causality.

In summary, the physical limitations on scattering and absorption discussed in Ref. 12 also hold for any metamaterials satisfying primitive causality. For a single frequency, metamaterials may possess extraordinary physical properties, but over any bandwidth they are with respect to scattering and absorption not different from materials with the eigenvalues of $\boldsymbol{\chi}_\mathrm{e}$ and $\boldsymbol{\chi}_\mathrm{m}$ non-negative.

4   Numerical synthesis of metamaterials

In this section, numerical results for three temporally dispersive scatterers are discussed in terms of the physical limitations in Sec. 3. The examples are chosen to provide a fictitious numerical synthesis of metamaterials. For convenience, the examples are restricted to isotropic material properties, $i.e.$, $\boldsymbol{\chi}_\mathrm{e} = \chi_\mathrm{e}\mathbf{I}$ and $\boldsymbol{\chi}_\mathrm{m} = \chi_\mathrm{m}\mathbf{I}$, where $\mathbf{I}$ denotes the unit dyadic. A similar example for the Lorentz dispersive cylinder is given in Ref. 12.

4.1   The Lorentz dispersive prolate spheroid

The averaged extinction cross section $\bar{\sigma}_\mathrm{ext}$ for a homogeneous and non-magnetic $(\chi_\mathrm{m} = 0)$ prolate spheroid with semi-axis ratio $\xi = 1/2$ is depicted in Fig. 1. The prolate spheroid is temporally dispersive with electric susceptibility given by the
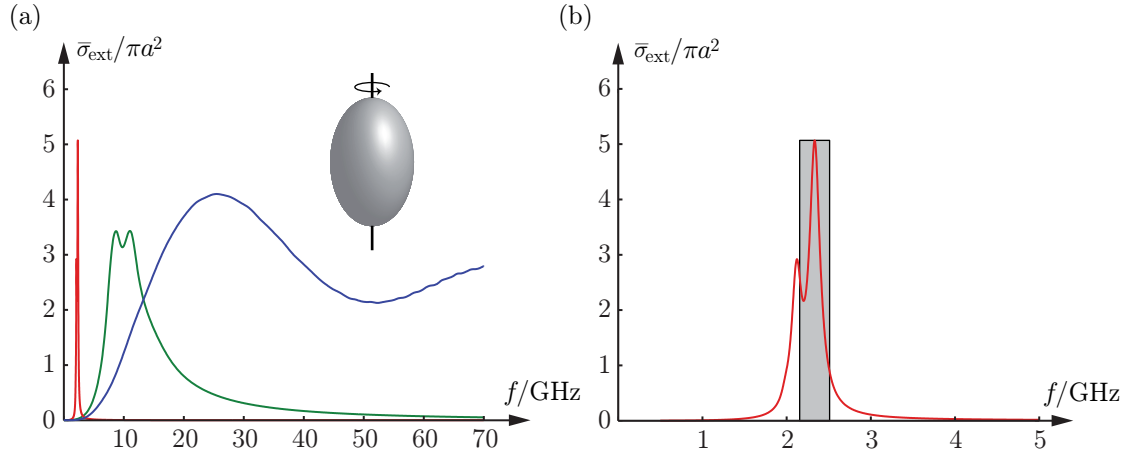
(a)

(b)

Figure 1: The averaged extinction cross section $\bar{\sigma}_{\text{ext}}$ as function of the frequency in GHz for a prolate spheroid with semi-axis ratio $\xi = 1/2$. Note the normalization with πa^2, where $a = 1\,\text{cm}$ denotes the radius of the volume-equivalent sphere.

Lorentz model, see Ref. 8,

$$\chi_{\text{e}}(\omega) = \frac{\omega_{\text{p}}^2}{\omega_0^2 - \omega^2 - \mathrm{i}\omega\nu},$$

where $(\omega - \omega_0)\,\text{Re}\,\chi_{\text{e}}(\omega) \leq 0$ and $\text{Im}\,\chi_{\text{e}}(\omega) \geq 0$ for $\omega \in [0,\infty)$. Explicit values of ω_{p}, ω_0 and ν for the two curves with peaks at $2\,\text{GHz}$ and $10\,\text{GHz}$ are $\omega_{\text{p}} = \omega_0 = 4\pi \cdot 10^9\,\text{rad/s}$, $\nu = 7 \cdot 10^8\,\text{rad/s}$, and $\omega_{\text{p}} = \omega_0 = 20\pi \cdot 10^9\,\text{rad/s}$, $\nu = 10^{10}\,\text{rad/s}$, respectively. The third curve in Fig. 1a corresponds to the non-dispersive case with $\chi_{\text{e}} = 1$, independent of ω. Since the three curves in Fig. 1a have the same values of χ_{e} in the long wavelength limit, *i.e.*, $\chi_{\text{e}}(0) = 1$, it follows from (2.5) that their integrated extinctions coincide.

Closed-form expressions of the averaged integrated extinction (2.6) exist for the prolate and oblate spheroids, see Ref. 12. For a non-magnetic spheroid with semi-axis ratio ξ,

$$\int_0^\infty \bar{\sigma}_{\text{ext}}(\lambda)\,\mathrm{d}\lambda = \frac{4\pi^3 a^3}{9} \sum_{j=1}^3 \frac{1}{1 + L_j(\xi)}, \tag{4.1}$$

where $L_j(\xi)$ denote the associated depolarizing factors and a is the radius of the volume equivalent sphere. For a prolate spheroid with semi-axis ratio $\xi = 1/2$, the depolarizing factors are approximately given by $L_1(1/2) = L_2(1/2) = 0.4132$ and $L_3(1/2) = 0.1736$, see Ref. 12. For the prolate spheroid in Fig. 1, $a = 1\,\text{cm}$, and the right hand side of (4.1) is equal to $31.24\,\text{cm}^3$. The integrated extinction $31.24\,\text{cm}^3$ is also numerically confirmed with arbitrary precision for the three curves in Fig. 1a.

Fig. 1b is a close-up of the $2\,\text{GHz}$ peak in Fig. 1a. The shaded box represents a realization of an artificial scatterer with the averaged integrated extinction $31.24\,\text{cm}^3$ centered around the peak. The integrated extinction for the boundary curve of the box and the three curves in Fig. 1a coincide. Note that the width of the box is
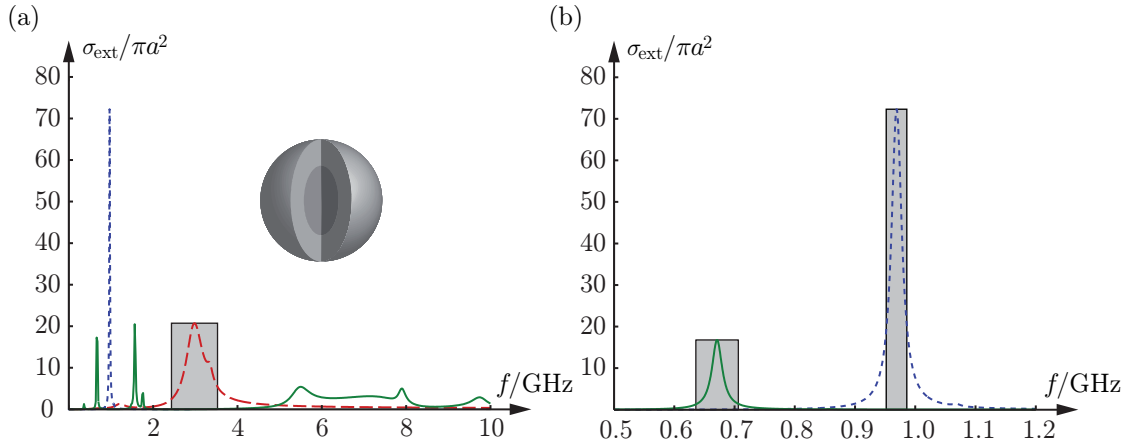
Figure 2: The extinction cross section σ_{ext} as function of the frequency in GHz for a stratified sphere which attains simultaneously negative values of the permittivity and the permeability. Note the normalization with the geometrical cross section πa^2, where $a = 1\,\text{cm}$ denotes the outer radius of the sphere.

approximately equal to the bandwidth of the peak when evaluated at half amplitude. The calculation in Fig. 1 is based on the implementation of the T-matrix approach in Ref. 6. For a similar example given by the Lorentz dispersive cylinder, see Ref. 12.

4.2 The Drude dispersive stratified sphere

The extinction cross section σ_{ext} for a stratified sphere with two layers of equal volume is depicted in Fig. 2. The stratified sphere is temporally dispersive with identical electric ($\ell = \text{e}$) and magnetic ($\ell = \text{m}$) material properties given by the Drude model

$$\chi_\ell(\omega) = \frac{\mathrm{i}\varsigma}{\epsilon_0\omega(1 - \mathrm{i}\omega\tau)}, \qquad \ell = \text{e, m}, \tag{4.2}$$

where $\varsigma > 0$ and $\tau > 0$. The real and imaginary parts of (4.2) read

$$\chi_\ell(\omega) = \frac{-\varsigma\tau}{\epsilon_0(1 + \omega^2\tau^2)} + \mathrm{i}\frac{\varsigma}{\epsilon_0\omega(1 + \omega^2\tau^2)}. \tag{4.3}$$

Since $\operatorname{Re}\chi_\ell(\omega) < 0$ for $\omega \in [0, \infty)$, the stratified sphere in Fig. 2 attains simultaneously negative values of the permittivity and the permeability. The calculation in Fig. 2 is based on a Möbius transformation applied to the classical Mie series expansion in Refs. 7 and 8.

The two curves in Fig. 2a with peaks at $0.97\,\text{GHz}$ (dotted line) and $3.0\,\text{GHz}$ (dashed line) correspond to a homogeneous sphere with identical material properties in the inner and outer layers. These two curves are characterized by the relaxation times $\tau = 10^{-8}\,\text{s}$ and $\tau = 10^{-9}\,\text{s}$, respectively, and with conductivity $\varsigma = 10\,\text{S/m}$ in both cases. For the third curve (solid line) with peaks at $0.67\,\text{GHz}$ and $1.6\,\text{GHz}$, the material parameters of the outer layer are $\tau = 8 \cdot 10^{-9}\,\text{s}$ and $\varsigma = 10\,\text{S/m}$, while the

inner layer is non-dispersive with $\chi_{e1} = 10$ and $\chi_{m1} = 0$ independent of ω. Fig. 2b provides a close-up of the peaks at $0.67\,\text{GHz}$ and $0.97\,\text{GHz}$.

Closed-form expressions of the electric polarizability dyadic $\boldsymbol{\gamma}_e$ exist for the stratified sphere, see Ref. 12. For a stratified sphere of two layers, the integrated extinction can be expressed as

$$\int_0^\infty \sigma_{\text{ext}}(\lambda)\,\mathrm{d}\lambda = 4\pi^3 a^3 \sum_{\ell=\text{e,m}} \frac{\chi_{\ell 2}(\chi_{\ell 1} + 2\chi_{\ell 2} + 3) + \zeta^3(2\chi_{\ell 2} + 3)(\chi_{\ell 1} - \chi_{\ell 2})}{(\chi_{\ell 2} + 3)(\chi_{\ell 1} + 2\chi_{\ell 2} + 3) + 2\zeta^3\chi_{\ell 2}(\chi_{\ell 1} - \chi_{\ell 2})}, \quad (4.4)$$

where a denotes the outer radius, and $\chi_{\ell 1}$ and $\chi_{\ell 2}$ represent the long wavelength susceptibilities of the inner and outer layers, respectively. Furthermore, $\zeta \in [0, 1]$ denotes the quotient between the inner and the outer radii.

Since (4.2) is characterized by a conductivity term which is singular at $\omega = 0$, the discussion above implies that the right hand side of (4.4) is subject to the limits $\chi_{e2} \to \infty$ and $\chi_{m2} \to \infty$. Based on this observation, it is concluded that the integrated extinction for the three curves in Fig. 2 coincide and are equal to $8\pi^3 a^3$ or $248.0\,\text{cm}^3$, where $a = 1\,\text{cm}$ has been used. In contrast to the limits $\chi_{e1} \to \infty$ and $\chi_{m1} \to \infty$, this result is independent of ζ as well as χ_{e1} and χ_{m1}. Note that (2.3) and (2.5) yield that the integrated extinction $8\pi^3 a^3$ is equivalent to the long wavelength limit $\varrho(0) = 2a^3$. The integrated extinction $248.0\,\text{cm}^3$ is numerically confirmed with arbitrary precision for the three curves in Fig. 2.

The physical limitation (3.3) is depicted by the shaded boxes in Fig. 2. These boxes correspond to artificial scatterers with extinction cross sections supported at the peaks $0.67\,\text{GHz}$, $0.97\,\text{GHz}$ and $3.0\,\text{GHz}$. The integrated extinction of each box is equal to $248.0\,\text{cm}^3$ and coincides with the integrated extinction for any other curve in the figure. From Fig. 2 it is seen how the width of the box increases as the peaks are suppressed in magnitude and shifted toward higher frequencies. Note that the tiny peaks at $0.36\,\text{GHz}$ (solid line) and $1.2\,\text{GHz}$ (dashed line) constitute a large part of the integrated extinction, thus implying that the peaks at $0.67\,\text{GHz}$ and $3.0\,\text{GHz}$ do not fit the boxes that well in comparison with the box centered at $0.97\,\text{GHz}$. Recall that the area of the boxes in Fig. 2 only depends on the properties of V in the long wavelength limit, and is hence independent of any temporal dispersion for $\omega > 0$.

The extinction cross section for a non-magnetic stratified sphere with two layers is depicted in Fig. 3. The stratified sphere is temporally dispersive with electric susceptibility χ_e given by the Drude model (4.2). The two curves in Fig. 3a with peaks at $0.96\,\text{GHz}$ (dotted line) and $2.7\,\text{GHz}$ (dashed line) correspond to the homogeneous case with identical material parameters in both layers: $\tau = 10^{-8}\,\text{s}$ and $\tau = 10^{-9}\,\text{s}$, respectively, with $\varsigma = 10\,\text{S/m}$ in both cases. For the third curve with peak at $1.4\,\text{GHz}$ (solid line), the material parameters of the outer layer is $\varsigma = 10\,\text{S/m}$ and $\tau = 10^{-8}\,\text{s}$, while the inner layer is non-dispersive with $\chi_{e1} = 10$ independent of ω. Fig. 3a is a close-up of the peaks at $0.96\,\text{GHz}$ and $1.4\,\text{GHz}$ with the associated box-shaped limitations.

Since the stratified sphere in Fig. 3 has the same electric long wavelength response as the scatterer in Fig. 2 but in addition is non-magnetic, it follows from (4.4) that
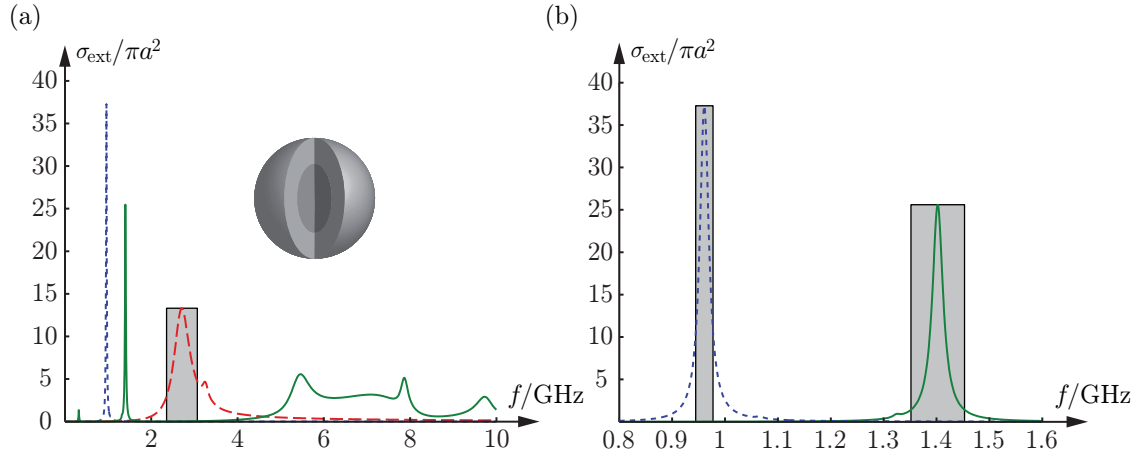
(a)

(b)

Figure 3: The extinction cross section σ_{ext} as function of the frequency in GHz for a non-magnetic stratified sphere which attain negative values of the permittivity. Note the normalization with the geometrical cross section πa^2, where $a = 1\,\text{cm}$ denotes the outer radius of the sphere.

the integrated extinction of the scatterer in Fig. 3 is half the integrated extinction of the scatterer in Fig. 2, *i.e.*, $4\pi^3 a^3$ or $124.0\,\text{cm}^3$. This observation is a direct consequence of the symmetry of (4.4) with respect to electric ($\ell = \text{e}$) and magnetic ($\ell = \text{m}$) material properties. The result is also supported by the fact that the amplitude of, say, the peak at $0.97\,\text{GHz}$ in Fig. 2 is approximately twice as large as the corresponding peak at $0.96\,\text{GHz}$ in Fig. 3.

5   Conclusions

The conclusions of the present paper are clear: independent of how the materials in the scatterer are defined and modeled by temporal dispersion (*i.e.*, irrespective of the sign of the permittivity and permeability), the holomorphic properties of the forward scattering dyadic imply that, from a broadband point of view, there is no fundamental difference in scattering and absorption between metamaterials and ordinary materials. For a single frequency, metamaterials may possess extraordinary properties, but with respect to any bandwidth such materials are no different from any other naturally formed substances as long as causality is obeyed. As a consequence, if metamaterials are used to lower the resonance frequency, this is done to the cost of an increasing Q-value of the resonance. The present analysis includes materials modeled by anisotropy and heterogeneity, and can be extended to general bianisotropic materials as well. For example, the introduction of chirality does not contribute to the integrated extinction since all chiral effects vanish in the long wavelength limit.

It is believed that there are more physical quantities that apply to the theory for broadband scattering in Ref. 12. Thus far, the theory has been applied fruitfully

to arbitrary antennas in Refs. 1 and 3 to yield physical limitations on antenna performance and information capacity. Similar broadband limitations on cloaking and invisibility using metamaterials and other exotic material models are currently under investigation.

Acknowledgment

References

[1] M. Gustafsson, C. Sohl, and G. Kristensson. Physical limitations on antennas of arbitrary shape. *Proc. R. Soc. A*, **463**, 2589–2607, 2007.

[2] M. Gustafsson. On the non-uniqueness of the electromagnetic instantaneous response. *J. Phys. A: Math. Gen.*, **36**, 1743–1758, 2003.

[3] M. Gustafsson, C. Sohl, and G. Kristensson. Physical limitations on antennas of arbitrary shape. Technical Report LUTEDX/(TEAT-7153)/1–37/(2007), Lund University, Department of Electrical and Information Technology, P.O. Box 118, S-221 00 Lund, Sweden, 2007. http://www.eit.lth.se.

[4] R. E. Kleinman and T. B. A. Senior. Rayleigh scattering. In V. V. Varadan and V. K. Varadan, editors, *Low and high frequency asymptotics*, volume 2 of *Acoustic, Electromagnetic and Elastic Wave Scattering*, chapter 1, pages 1–70. Elsevier Science Publishers, Amsterdam, 1986.

[5] L. D. Landau, E. M. Lifshitz, and L. P. Pitaevskiĭ. *Electrodynamics of Continuous Media*. Pergamon, Oxford, second edition, 1984.

[6] M. I. Mishchenko and L. D. Travis. Capabilities and limitations of a current FORTRAN implementation of the T-matrix method for randomly oriented, rotationally symmetric scatterers. *J. Quant. Spectrosc. Radiat. Transfer*, **60**(3), 309–324, 1998.

[7] R. G. Newton. *Scattering Theory of Waves and Particles*. Springer-Verlag, New York, 1982.

[8] H. M. Nussenzveig. *Causality and dispersion relations*. Academic Press, London, 1972.

[9] S. A. Ramakrishna. Physics of negative refractive index materials. *Reports on Progress in Physics*, **68**(2), 449–521, 2005.

[10] R. Ruppin. Extinction properties of a sphere with negative permittivity and permeability. *Solid State Commun.*, **116**, 411–415, 2000.

[11] D. R. Smith, J. B. Pendry, and M. C. K. Wiltshire. Metamaterials and negative refractive index. *Science*, **305**(5685), 788–792, 2004.

[12] C. Sohl, M. Gustafsson, and G. Kristensson. Physical limitations on broadband scattering by heterogeneous obstacles. *J. Phys. A: Math. Theor.*, **40**, 11165–11182, 2007.

[13] H. van de Hulst. *Light Scattering by Small Particles.* John Wiley & Sons, Inc., New York, 1957.

[14] V. G. Veselago. The electrodynamics of substances with simultaneously negative values of ϵ and μ. *Sov. Phys. Usp.*, **10**(4), 509–514, 1968.